Oral Presentation

The 7th TSME International Conference on Mechanical Engineering
13-16 December 2016

TSME ICOME 2016
Mechanical Engineering Innovation for Green Society

AME0018

Conceptual Design of Fixed Wing-VTOL UAV for AED transport

Watcharapol Saengphet[1], Chalothorn Thumthae[2,*]

[1] Mechanical Engineering, Suranaree University of Technology, Nakhon Ratchasima, 30000, Thailand
[2] Mechanical Engineering, Suranaree University of Technology, Nakhon Ratchasima, 30000, Thailand
[*] Corresponding Author: E-mail chalothorn@sut.ac.th, Telephone Number 0-4422-4556

Abstract

This study presents the conceptual design of fixed wing battery-powered UAV, designed to carry an Automated External Defibrillator (AED) or any 1.5 kg of payload. This aircraft has ability, not only to take-off, landing or hover as multirotor aircraft but also to cruise similar to the fixed wing aircraft leads to reach the high speed and endurance without additional rotor-tilting mechanism. The new UAV type is called the hybrid UAV. Follow by the hybrid UAV concepts, the design process was initiated by estimating maximum take-off weight. Battery weight and capacity were then estimated from fixed wing and multirotor power required. Moreover, the subsystem of propulsion including propeller, coaxial rotor, motor, ESC and battery were reviewed and discussed. Constant power method was adopted to improve accuracy of the range and the endurance estimation of battery-powered aircraft instead of constant voltage method. In order to match the mission requirements and obtain the design space, the preliminary sizing was established. Computational fluid dynamics is not yet studied in this work. Finally, the conceptual design results, the effect of takeoff velocity to energy consumption and energy management were presented and consulted.

Keywords: Conceptual design, Hybrid UAV, VTOL, battery-powered UAV, Constant power method

1. Introduction

Unmanned Aerial Vehicle (UAV) have been widely used and become very popular application such as Traffic monitoring [1] reconnaissance and surveillance [2]. UAV is typically categorized into 3 group consists of fixed wing, multirotor and hybrid UAV. The largest fraction fixed wing lift is created by its wing, propeller produces thrust to maintain speed in order to fly straight and level. Flight speed, range and endurance are its advantage. However, takeoff and landing distance are required. Examples off fixed wing in conventional configuration: Raven [3], Skylite-B [4]. The Tailless (flying wing) configuration: ZALA 421-04M [5], ITU tailless [6]. Multirotor's lift is created from propeller thrust. Due to its high ability in vertical takeoff and landing (VTOL), so the multirotor can be operated certain missions such as observing the interesting target using altitude and position hole which was unable by the fixed wing. Moreover, it requires relatively small ground area for operation. However, its drawbacks are endurance and speed.

In order to combine the advantages and overcome the problems, Hybrid UAV is created. Hybrid UAV was categorized into 2 main type, convertiplane and Tail-sitter [7]. A convertiplane was categorized into 4 subtypes, including tilt-rotor, tilt-wing, rotor-wing and dual system. The advantage of tilt-rotor and tilt-wing was achieved by using their motor effectively because motors were used for both vertical and horizontal flight. However, motor or wing tilting mechanism require complicated software and hardware. Stability during transition flight is a critical point which may lead to the catastrophe. For example, the TURAC [8], and the Firefly6 [9].

A Dual system separated motor for vertical and horizontal flight. Both software and hardware were intended to simplify by this concept. Consequently, controller and mechanism are relatively simpler than tilting platform. The extra weight and drag from unused rotor and motor were resulted in the increasing of power required during the horizontal flight (fixed wing flight mode) and increasing the capacity of battery, thus total weight were increased, for examples: Amazon Prime Air [10] and Canberra [11].

On the other hand, a Tail-sitter is an aircraft that land by its tail. Transition from vertical to horizontal mode and vice versa were performed (tilt body) by its control surfaces or motors (differential thrust). This concept intended to reduce weight from the tilting system or dual system. However, stronger tails were required. Since its body was oriented vertically during VTOL mode, tail-sitter is more vulnerable to wind. Consequently, complicated control system was required, such as VertiKUL [12], ITU Tail-sitter [13].

2. Background and requirements

Nowadays, UAVs are becoming a trendy and common vehicle in medical application (Fig. 1) [14], [15]. Due to their capability, the carried object such as AED, drugs, other medical tools and samples could be delivered to the target using GPS/INS navigation or remotely pilot system to avoid traffic jam. Moreover, UAV is able to land on the top of the high building or even of the small field, thus it can reduce the response time. Every minute that passed without CPR and defibrillation, there is a 10% drop in chance of survival [14]. This was the critical issue that need to be solved.

According to National Institute for Emergency Medicine annual report 2014 [16], the emergency team must reach the patient or target within 8 minutes. Furthermore, the main reason of the high number of casualties is the long-delaying response time of emergency service.

Therefore, this work was aimed to design an UAV for AED transport mission. Regarding to the previous review, the combination of multirotor and fixed wing, a hybrid UAV, were an expected platform. The details of hybrid UAV were discussed in the general and mission requirements section. The conceptual design process was established to sketch, analyze and select the appropriate platform in order to match the mission. Appearance and performance of aircraft depend on general and mission requirements.

(a) (b)

Fig. 1 TU Delft (a) [14] and Vayu (b) [15]

2.1 General requirements

The general requirement that applied for this aircraft consist of reliability, maintainability, availability and transportability (RMAT concept) as shown in Fig. 2. RMAT can be explained more details as follows.

Since the most critical reliabilities are engine and software control (firmware). Non-tilting rotor system was selected. Furthermore, non-tilting rotor indicate also maintainability because of less moving parts and mechanisms. Downtime, preventive and collective maintenance must be considered. Availability is the probability that a system is operable and ready to perform its intended mission at any given time in the specified operational environment. However, this ability is affected by maintainability [17]. The transportability is the capability of the system to be moved by towing, self-propulsion, or carrier. UAV concept is able to reassembly or folding the wing/motor according to transportability. (detail of the reassembly concept was not discussed in this study.)

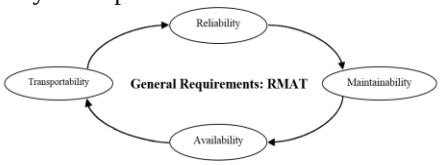

Fig. 2 General requirements

2.2 Mission requirements

As known, using UAV in the city is unsafe. Datalink loss is one of the most critical issue since the radio signal is blocked by buildings. Increasing the distance from ground control station (GCS), decreasing in the signal strength. In this state of design, the communication problems and how to address them will not be discussed. In order to avoid the risk from signal loss, the maximum operating range is set to 5 km and operating altitude is 150 m above ground level. Cruise speed for stand mission (low headwind magnitude) is 20 m/s in order to reach the target within 8 minutes. According to the safety concern, loiter time for fixed wing flight is 5 minutes and for multirotor flight is 2 minutes. The other parameters were shown in Table. 1. Energy consumption was calculated based on the mission profile as Fig. 3.

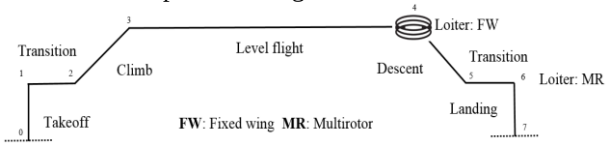

Fig. 3 Standard mission profile

Table. 1 Mission requirements parameters

Mode	*Requirement*	*Value*	*Description*
MR	V_{TO}	3 m/s	Takeoff velocity
	V_{LD}	2 m/s	Landing velocity
	H_{TO}	50 m	Takeoff altitude
	H_{LD}	30 m	Landing altitude
	t_{tran}	10 s	Transition time
	t_{hold}	2 mins	Position hold
FW	V_{cruise}	20 m/s	Cruise to target
	ROC	5 m/s	Max. climb rate
	S_{range}	5 km	Operating range
	H_{cruise}	150 m	Cruise altitude
	t_{loiter}	5 mins	Loiter time

3. Conceptual Design

Conceptual design plan shown in Fig. 4 consist of 6 subsections: maximum takeoff weight buildup, battery weight estimation, drag estimation, power and energy consumption and subsystem efficiency.

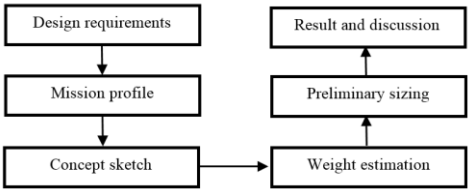

Fig. 4 Conceptual design plan

3.1 Concept sketch

According to the general and mission requirements, the concept of aircraft concluded as:

1. Tailless (flying wing): To reduce moving parts. Tail boom as the conventional configuration was suffered from cross wind during VTOL. It is difficult to control heading especially in automatic flight.

2. Y6-coaxial rotor: To improve aircraft compactness and provide enough thrust.

3. Single tractor propeller: To install Y6 rotor, the easiest way to install fixed wing propeller is tractor.

4. Retractable landing gear: To reduce drag.

5. Payload placement: On the top of fuselage (Fig. 5), red cross medical symbol.

AME0018

The major challenges for hybrid UAV is decreasing in aerodynamic efficiency and increasing in takeoff weight thus resulted in increasing in the energy consumption. At the same payload weight this UAV may has a large wing area. The expected flight time is between multirotor and fixed wing. However, the high speed cruise cause the high energy consumption thus shorten flight time.

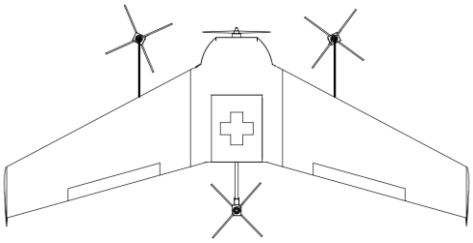

Fig. 5 Concept sketch of flying wing-Y6

3.2 Maximum takeoff weight buildup

There are many different techniques for weight estimation. If historical data exists, it quite well to use that. However, if do not, another technique will be used instead. Weight Estimating Relationships (WERs) were generally described in literatures such as Roskam [18]. Since it was not applicable for mini UAVs (1 to 20 kg) [19]. Therefore, new WERs is employed [1]. The logarithmic relation of empty weight is written as:

$$W_e = 10^{-0.155+0.911\cdot\log_{10}(W_{TO})} \quad (1)$$

Eq. (1), the maximum takeoff weight was required as input to estimate the empty weight. Therefore, iterative weight process is adopted as shown in Fig. 6.

The maximum takeoff weight was broken up into 4 elements: empty weight, payload weight, multirotor system weight and battery weight as Eq. (2).

$$W_{TO} = W_e + W_{pl} + W_{MR} + W_b \quad (2)$$

Since the WERs did not take the hybrid UAV weight into the database, multirotor system weight was set as a part of payload during iteration. The empty weight includes the structural weight, the fixed wing propulsion system weight, and the fixed equipment weight. Multirotor system weight includes motor, ESC, propeller and motor arms.

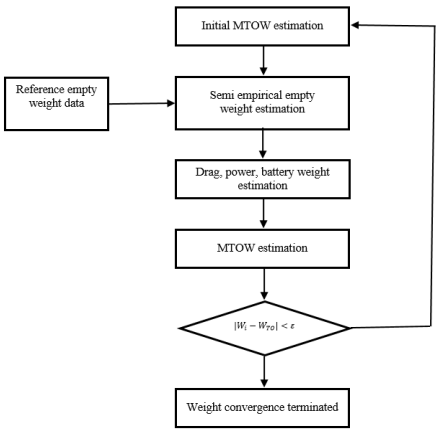

Fig. 6 Iterative weight process

3.3 Battery weight estimation

In general, battery is estimated from estimated energy required (Wh) divided by mass specific energy density (Wh/kg) [8, 12]. In order to improve estimation accuracy, Lithium-Polymer battery weight models was employed and found [20-22]. Quadratic Model [22] is adopted due to its large number of database, thus reliability.

$$E_B(Wh) = 4.04(m_B)^2 + 139m_B + 0.0155 \quad (3)$$

UAV requires a constant power not constant current. Therefore, the constant power method was utilized in order to increase the accuracy of range and endurance estimation for non-constant discharge rate [23]. This method converts constant current discharge curves which is a standard testing procedure to constant power discharge curves. Eqs. (4) – (6) were used, value of $i^nV(D)$ was obtained from tested data [23].

$$V_j = \left(\frac{i^nV(D)_{j-1}}{P_e^n} \right)^{1/(1-n)} \quad (4)$$

$$i_j = \frac{P_e}{V_j} \quad (5)$$

$$D_j = i_j \cdot (\Delta t) + D_{j-1} \quad (6)$$

Where: n=0.05, P_e is electric power (W) and Δt is time step (h). D is discharged capacity (mAh).

Each capacity has its own characteristic. Therefore, pre-estimation capacity, Eq. (3), is need to identify and select the proper capacity.

Table. 2 General parameters

Parameter name		*Value*
Reference area	S_{ref}	0.8 m^2
Maximum lift coefficient	$C_{L,\max}$	1
Air density at sea level	ρ_{SL}	1.225 kg/m^3
Air density at 150 m	ρ_{150}	1.198 kg/m^3

3.4 Drag estimation

A low subsonic speed aircraft as UAVs, the drag was built up from lift independent drag, the zero-lift/parasite drag and lift dependent drag, induced drag and parasite drag due to change in angle of attack [24]. Total drag shown as Eq. (7).

$$C_D = C_{D0} + \frac{C_L^2}{e\pi AR} \quad (7)$$

3.4.1 Zero-lift/parasite drag

This drag component was affected by viscosity. The main components are skin friction drag, pressure drag and interference drag [1]. Component buildup method was employed to calculate the parasite drag as Eq. (8) [25].

$$C_{D_0} = 1.1\left(\frac{\sum_{i=1}^{n} C_{f_i} FF_i Q_i S_{wet_i}}{S_{ref_i}} + C_{D_{MR}}\right) \quad (8)$$

A number 1.1 is to account leakage and protuberance drag. This type of drag is difficult to predict. First term of the right hand side in the bracket is the summation of drag due to wing, winglets external store and fuselage. C_f represents skin friction coefficient from flat plate which depend on Reynolds number and skin roughness. Friction coefficient for laminar and turbulent flow [26] are expressed as:

$$C_{f_{tr}} = \frac{0.074}{\mathrm{Re}^{0.2}}. \qquad \mathrm{Re}<10^6 \quad (9)$$

According to the tractor propeller, the velocity increase, thus Reynolds number. To account this drag increment the followings equations are presented [27]:

$$\Delta V = \left(\frac{2}{\eta_{prop}} - 2\right) V_\infty \quad (10)$$

Form factor, FF presents the drag correction due to pressure drag and airfoil/fuselage thickness. Both wing and fuselage, there are several existing models such as [26, 28]. The comparison of these models were presented in [29]. In this work, form factor model of wing Raymer [25] and fuselage from Hoerner [26] were utilized.

$$FF_{wing,winglet} = \left[1 + \frac{0.6}{(x/c)}\left(\frac{t}{c}\right) + 100\left(\frac{t}{c}\right)^4\right] \cdot \left[1.34M^{0.18}(\cos\Lambda_m)^{0.28}\right] \quad (11)$$

$$FF_{fuselage,store} = 1 + 1.5\left(\frac{d^*}{l^*}\right)^{\frac{3}{2}} + 7\left(\frac{d^*}{l^*}\right)^3 \quad (12)$$

$$\frac{l^*}{d^*_{eq}} = 2\left(\frac{l^*}{b^* + h^*}\right) \quad (13)$$

Interference factor, Q is used to account aerodynamic interference between components. These value can be seen in Table. 3.

Table. 3 Interference factor

Parameter name	*Value*
Q_{wing}	1
$Q_{fuselage}$	1.2
$Q_{winglet}$	1.04

Stopped rotor drag was calculated from the same method that used to determine the drag over feathered propeller [26] as Eq. 14. Drag coefficient of feathered propeller (2 blades) is approximately 0.1.

$$C_{D_{prop}} = \frac{C_{D_{prop}}(NDC_{0.7R})}{S_{ref}} \quad (14)$$

Motor shape is assumed to be circular cylinder and predicted by Eq. (15). Drag coefficient is 1.2 and reference area of motor is the length multiplied by diameter.

$$C_{D_{motor}} = \frac{C_{D_{motor}}(l_{motor} D_{motor})}{S_{ref}} \quad (15)$$

3.4.2 Induced drag

Assume the non-elliptical lift distribution and parasite drag due to change in angle of attack are accounted by Oswald's span efficiency factor which is model of swept wing from [25].

$$C_{Di} = \frac{C_L^2}{\pi e AR} \quad (16)$$

$$e = 4.61\left(1 - 0.045AR^{0.68}\right)(\cos\Lambda_{LE})^{0.15} - 3.1 \quad (17)$$

Note that, if angle of attack increase, the drag may increase than expectation. Because of increasing in multirotor-propeller induced drag. However, this effect can be neglected if the wings were installed at the proper incident angle and propeller attached parallel to the longitudinal axis of fuselage.

3.4.3 Wetted area

Wetted area is the area that is exposed to the flow. For wing, winglet and fuselage are approximated as follows [25]:

$$S_{wet_{wing}} \approx 2\left(1 + 0.2\frac{t}{c}\right) S_{ref} \quad (18)$$

$$S_{wet_{fuselage}} \approx \frac{3.4\left(S_{f,top} + S_{f,side}\right)}{2} \quad (19)$$

Table. 4 Wing and winglet parameters

Parameter name		*Wing*	*Winglet*
Leading edge swept, degree	Λ_m	20	35
Max. thickness to chord ratio	t/c	0.12	0.09
Max. thickness position to chord	x/c	0.25	0.3
Root chord, m	c_r	0.5	0.25
Taper ratio	λ	0.5	0.5
Aspect ratio	AR	5	1

Noted that the wing parameters estimate from typical reflex airfoil and wingtip from NACA0009, Aspect ratio, taper ratio and swept angle were selected from previous references aircraft: ITU Tailless [6] and TURAC [8].

Table. 5 Fuselage and external store parameters

Parameter name		*Fuselage*	*Store*
Length, m	l^*	0.6	0.3
Width, m	b^*	0.3	0.25
Height, m	h^*	0.15	0.10

Noted that the external store dimension is estimated from AED cover case.

Table. 6 Multirotor parameters

Parameter name		*Value*
Number of rotor	N	6
Propeller diameter	D_{prop}	15 in
Chord at 0.7R	$C_{0.7R}$	0.038 m
Motor + Prop weight	W_{motor}	0.1 kg/unit
ESC weight	W_{esc}	0.003 kg/unit
Motor length	l_{motor}	0.028 m
Motor diameter	D_{motor}	0.042 m

Noted that reference motor is Tiger motor MN3510, 700 KV.

3.5 Power required and energy consumption

Power required for this UAV is divided into fixed wing and multirotor power required.

3.5.1 Fixed wing power required

According to the mission profile, the fixed wing flight mode consists of cruise to target (C2T), loiter, cruise back to base (C2B). After total drag coefficient was estimated, estimated drag polar was plotted. Minimum power required and minimum thrust required velocity are expressed as [24].

Minimum drag velocity:

$$V_{D_{\min}} = \sqrt{\left(\frac{W_{TO}}{S_{ref}}\frac{2}{\rho_{150}}\frac{1}{\sqrt{C_{D0}\cdot\pi\cdot e\cdot AR}}\right)} \quad (20)$$

Minimum power required velocity:

$$V_{P_{\min}} = \sqrt{\left(\frac{W_{TO}}{S_{ref}}\frac{2}{\rho_{150}}\frac{1}{\sqrt{3\cdot C_{D0}\cdot\pi\cdot e\cdot AR}}\right)} \quad (21)$$

3.5.2 Multirotor power required

The power required of rotorcraft was derived based on momentum theory on rotor disk [30]. The takeoff thrust required and power required of each propeller are expressed [31]:

$$T_{TO} = \frac{\left(W_{TO} + \frac{1}{2}\rho_{SL}V_{TO}^2 S_{ref} C_{D0_{axial}}\right)}{\eta_{coaxial} N} \quad (22)$$

$$P_{TO} = \frac{T_{TO}V_{TO}}{2FM}\left[2+\sqrt{1+\left(\frac{2T_{TO}}{\rho_{SL}A_{prop}V_{TO}^2}\right)}\right] \quad (23)$$

$C_{D0_{axial}}$ is drag coefficient in axial climb, assume to be flat plate, 1.9 (10^4 < Re < 10^5) [26]. N is number of rotor, $\eta_{coaxial}$ is coaxial thrust efficiency, FM is figure of merit and A_{prop} is propeller disk area.

Hover power required for each rotor and hover induced velocity are expressed as:

$$P_H = \frac{\left(\frac{W_{TO}}{\eta_{coaxial}N}\right)^{\frac{3}{2}}}{FM\cdot\sqrt{2\cdot\rho_{SL}\cdot A_{prop}}} \quad (24)$$

$$V_H = \sqrt{\frac{(W_{TO}/\eta_{coaxial}N)}{2\rho_{SL}A_{prop}}} \quad (25)$$

In axial descend case, axial climb model (Eq. (27)) is not valid anymore since the rotor disk works in the vortex ring state (VRS) that exist for the case of descent velocity is less than 2 times of hover induced velocity ($V_{LD} \le 2V_H$). Consequently, the descent induced velocity was estimated as a quadratic curve from experimental data. Landing power required are expressed as:

$$V_i = V_H\begin{pmatrix}1.2 - 1.125x - 1.372x^2 - 1.718x^3\\ -0.655x^4\end{pmatrix},$$

$$x = -\frac{V_{LD}}{V_H} \quad (26)$$

$$T_{LD} = \frac{\left(W_{TO} - \frac{1}{2}\rho_{SL}V_{TO}^2 S_{ref} C_{D0_{axial}}\right)}{\eta_{coaxial}N} \quad (27)$$

$$P_{LD} = \left(\frac{T_{LD}}{FM}\right)(V_i - V_{LD}) \quad (28)$$

3.5.3 Energy consumption

After power required was established, it was converted to electric energy required (Wh) by taking subsystem efficiency into account which was discussed in section 3.6 Subsystem efficiency.

The energy consumption of subsystem devices such as camera, radio, controller board are neglected.

Cruise:

$$C_{C2T} = \frac{S_{range}P}{V_{cruise}\eta_{tot,FW}3600} \quad (29)$$

Loiter:

$$C_{Loiter} = \frac{t_{loiter}P_{loiter}}{\eta_{tot,FW}3600} \quad (30)$$

Climb:

$$C_{Climb} = \frac{\eta_{prop}t_{climb}P_{climb}}{\eta_{tot,FW}3600} \quad (31)$$

Noted that the climb power would be selected from design space, power loading, in section 4.

Preliminary. design. η_{tot} represents the total efficiency consist of ESC, motor and propeller efficiency.

Multirotor:

$$C_{MR} = \frac{t_{MR} P_{MR} FM}{\eta_{tot,MR} 3600} \quad (32)$$

For Multirotor flight modes, the same equations were used to calculate energy required depend on time and power. The propeller efficiency is changed to figure of merit, FM.

The total energy required is expressed as Eq. (33). According to the safety concern, total energy required is divided by factor 0.7 to account the unpredicted voltage drop during discharging and cut-off voltage at low capacity. The validity of this value will be discussed later.

$$C_{tot} = \frac{C_{C2T} + C_{Loiter} + C_{Clmb} + C_{C2B} + C_{MR}}{0.7} \quad (33)$$

The result from Eq. (33) was passed onto Eq. (3) to do pre-estimation of battery weight before using power constant method [23] to recalculate range and endurance again. Moreover, the result from Eq. (33) was divided by nominal voltage (3.7 V per cell of LiPo battery) to obtain battery capacity. This is called constant voltage method.

3.6 Subsystem efficiency

In the conceptual design process, the efficiencies need to be estimated from existing literatures and manufacturer in order to reduce erroneous results. The propulsion components consist of propeller, coaxial rotor, motor, electronic speed control (ESC). The total efficiency of fixed wing and multirotor propulsion shown in Fig. 7 and are expressed as:

$$\eta_{tot,FW} = \eta_{esc} \eta_{motor} \eta_{prop} \quad (34)$$

$$\eta_{tot,MR} = \eta_{esc} \eta_{motor} FM \quad (35)$$

Fig. 7 Conversion of battery power to available propulsive power [32]

3.6.1 Propeller

Fixed wing and multirotor propeller have different shape. Blade width and blade angle or propeller pitch were optimized to match the operating condition.

Literature [33-35] investigated the fixed wing propeller with the diameter ranging from 10 – 13 inch and pitch 4.7 – 8 inch. Maximum efficiency was varied between 0.6 – 0.75 depend size, pitch and airfoil used.

Efficient rotor such as large scale aircraft typically has a FM between 0.7 – 0.8 [30]. Small-scale propeller can be found in [36]. Propeller size ranging from 2.25 – 5 inch shown relatively poor performance with the efficiency between 0.38 – 0.61. The larger diameter has more efficiency. Additionally, lower pitch at the same size has more efficiency. However, these size are too small for this aircraft. The larger diameter (more than 10 inch) test could not found. It is expected that the maximum efficiency would be more than 0.6.

3.6.2 Coaxial rotor

The disadvantage of coaxial rotor is thrust loss due to aerodynamic interference between rotors, thus rotor spacing and key parameters which contribute to coaxial rotor thrust efficiency must be reviewed. The different rotor spacing was tested with 200 mm of diameter [37]. The results shown that rotor spacing between 60 mm to 80 mm was achieved better performance and reached a constant value if the higher space was used. This result is consistent with [38] that the coaxial thrust was less than the sum of two isolated rotors. Literature [37] found that thrust loss was about 10%. However, [38] reported that 20%, rotor space was not found but can be estimated from motor length data that is in range of 52 to 60 mm. Within this range, the rotor might be reduced.

3.6.3 Motor

Traditional motor (brush DC) has widely used to predict motor performance. However, the result from testing [39] shown that this model did not accurately capture brushless motor (BLDC). If motor parameters are correct, the level of accuracy can be improved. The highest measured efficiency is 0.78 from 7 different bands. However, the result cannot be concluded that every bands have low motor efficiency. According to manufacturer data [40], motor efficiency varied from 0.8 to 0.95 depend on technology used, specification and operating condition such as propeller size, voltage supply and RPM.

3.6.4 Electronic speed control (ESC)

ESC efficiency was affected by resistive losses in electronic and FETs as well as loss due to duty cycle [32]. At normal operating condition as cruise which often set the throttle level (duty cycle) around 40% to 60%, within this range the efficiency is drop from nearly 1 at 100% duty cycle to 0.85 to 0.9 [32]. This result is consistent with [41], at the input voltage 14.8V ESC efficiency ranging from 0.8 to 0.9.

Subsystem efficiency for normal operating condition was shown in Table. 7.

Table. 7 Subsystem efficiency

Efficiency		***Value***
FW propeller	η_{prop}	0.70
Motor	η_{motor}	0.8
ESC	η_{esc}	0.9
MR propeller	FM	0.65
Coaxial rotor	$\eta_{coaxial}$	0.9
FW total	$\eta_{tot,FW}$	**0.50**
MR total	$\eta_{tot,MR}$	**0.47**

4. Preliminary sizing

In order to match the requirements and obtain design space, power loading (W/P) versus wing loading (W/S) diagram was established. 5 cases from fixed wing flight consist of stall, cruise back, climb rate, climb gradient were analyzed. The others would not be considered since those are not significant cases according to mission requirements.

Stall speed sizing:

$$\left(\frac{W}{S}\right)=\frac{1}{2}C_{L,\max}\rho_{150}V_s^2 \quad (36)$$

Cruise back (maximum range) sizing:

$$\left(\frac{W}{S}\right)=\frac{1}{2}\rho_{150}V_{C2B}^2\sqrt{\pi eARC_{D_0}} \quad (37)$$

Rate of climb sizing:

$$\left(\frac{W}{P}\right)=\frac{\eta_{prop}}{ROC+\sqrt{\frac{W}{S}\frac{2}{\rho_{150}}\frac{\sqrt{C_{D_0}}}{1.808(eAR)^{3/2}}}} \quad (38)$$

Climb gradient sizing:

$$\left(\frac{W}{P}\right)=\frac{\eta_{prop}}{\left(\frac{ROC}{V_{cruiseback}}+\frac{2C_{D_0}}{C_{L_{\max}}}\right)\sqrt{\frac{W}{S}\frac{2}{\rho_{150}}\frac{1}{C_{L_{\max}}}}} \quad (39)$$

The lowest wing loading and corresponding power loading (intersection of these 2 lines) will be selected to maintain the mission requirements.

5. Result and discussion

5.1 Zero lift drag

Aerodynamic optimization is the future work, therefore the assumption is wing, winglet and fuselage are appropriate dimension which are constant except the wing area. The zero lift drag was shown in Table.8

To maintain the mission requirements, drag coefficient from turbulent skin friction coefficient model was used to calculate energy consumption. Even this might lead to overestimation but at least, the mission is complete.

Table. 8 Zero lift drag of each model

Fixed wing	*Multirotor*	*Total*
0.025	0.021	0.051*

*Noted that sum of FW and MR drag coefficient is multiplied by factor 1.1 as Eq. (8).

The largest source of drag was obtained from wing, 30% of total drag (Fig. 8). Motor and propeller drag are in the same level, 23-24%. Fixed wing zero lift drag is 0.025 and multirotor drag is 0.047 as Table. 8. 54.4% of zero lift drag was obtained from fixed wing and 45.6% of multirotor drag (Fig. 9). The extra drag from multirotor system dramatically affects the fixed wing performance cause much energy is consumed. However, if the rotors aligned with air flow the total would decrease. Accuracy of multirotor drag was not discussed here. However, the result indicated that it could not be neglected and would be validated in the future work.

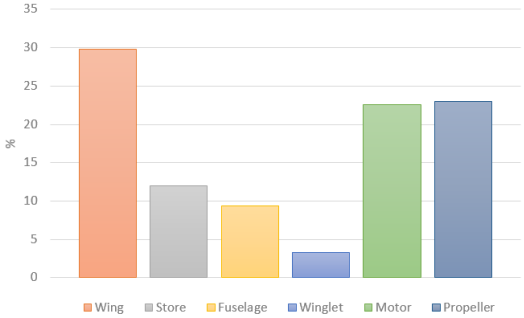

Fig. 8 Drag fraction of each component

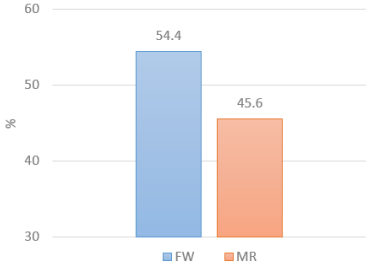

Fig. 9 Drag fraction of between fixed wing and Multirotor

5.2 Design space and initial sizing

The design space is shaded area (red) as figure 10. Before investigating in deep about the multirotor performance, selected wing loading (W/S) and power loading (W/S) are 88.2 N/m^2 and 0.11 respectively. The initial and new weights were shown in Table. 9. The empty weight from Eq. (1) is 34.20 N which seems higher than the reference aircraft [6]. This affect the multirotor energy consumption. The erroneous result occurs due to lack of database to derive the empirical equation. Additionally, the material played a critical role to structural weight. Therefore, the new empty weight (exclude multirotor motors) is set to 3 kg (29.43 N).

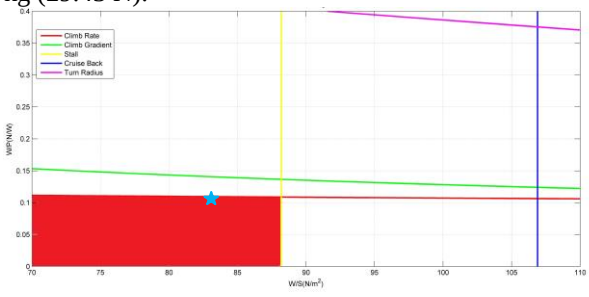

Fig. 10 Design space

Table. 9 General parameters

Parameter name		*Value*
Reference area	S	0.8 m^2
Power loading	W/P	0.11 N/W
Wing loading	W/S	83.36 N/m^2
Empty weight	W_e+W_{MR}	35.5 N

AME0018

Battery weight	W_b	16.48 N
Takeoff weight	W_{TO}	66.69 N
Battery capacity	C_b	15000 mAh

Battery capacity estimated by constant voltage method is about 15,000 mAh. Commercial off the shelf (COTS) battery have various capacity sizes. In order to use the power constant method [23] to verify the battery capacity obtained from Eq. (33), 3 packs of 5,000 mAh 4S battery were used and its characteristic appear in [23]. The effective capacity was set to 4,000 mAh to avoid voltage drop region.

Figs. 10– 11, maximum takeoff weight is 66.69 N (6.80 kg), The minimum drag speed is 13.1 m/s. Minimum power required speed is 10 m/s which is lower than the stall speed, thus 16 m/s is used both loiter and cruise back mode (approximately $1.2V_s$).

Lift to drag ratio of hybrid UAV is relatively low (Fig. 12) due to extra drag from multirotor system. This drag affects the energy consumption during fixed wing mission.

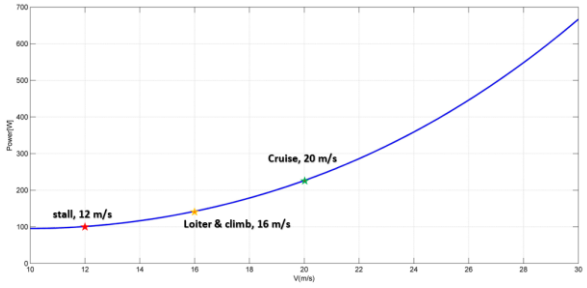

Fig. 10 Power required and airspeed

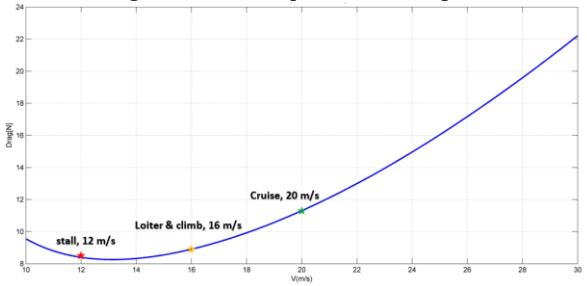

Fig. 11 Thrust required and airspeed

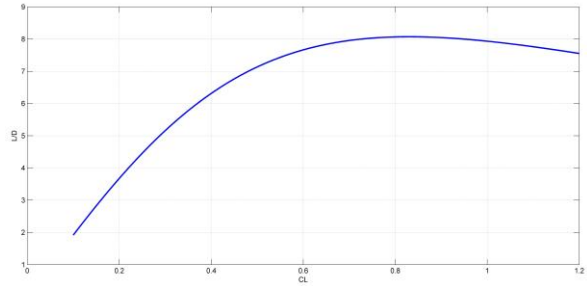

Fig. 12 Lift coefficient and lift to drag ratio

5.3 Power constant method result

According to Fig. 13, total energy required (Eq. (33)) divided by factor 0.7 seems well. Since the estimated battery weight and capacity by constant voltage method is able to achieve the mission which used the power constant method. The reasons lead to obtain erroneous result consists of underestimated drag, lower-than expected effective capacity, decrease in propeller, rotor, ESC and motor efficiency. Strong headwind could reduce the flight time in case of maintain ground speed.

The different number means different flight mode. The procedure starts from (1) takeoff, (2) transit (3) climb, (4) cruise, (5) loiter 2.5 mins., (6) transit+hover 1 mins., (7) land, (8) cruise back. The average current drain shown in Table. 10.

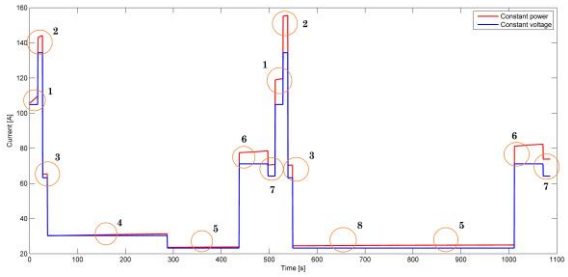

Fig. 13 Current drain during mission

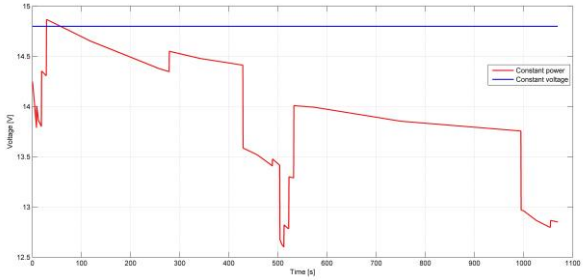

Fig. 14 Voltage drop due to current drain

The difference between constant voltage method and constant power method voltage is clear at high discharged capacity (cruise back to base region) and high current drain. During high power required, thus high current drain. The critical voltage drop region is transition to fixed wing. Minimum voltage drop region is loiter and cruise back.

In the vicinity of landing, voltage dropped lower than 13 V which was close to the critical or cutoff voltage which must be avoided. To address this problem, battery capacity should be added. However, propeller size must match the thrust required especially takeoff in order to achieve the desired vertical takeoff velocity.

Table. 10 Estimated current drain of each flight mode

Parameter name	***Current (A)***	
	B2T	***T2B***
Takeoff	105	112
Transition	144	155
Climb	65	70
Cruise	30	25
Loiter	23	25
Hover	78	82
Land	72	75

The largest energy consumption fraction is cruise and cruise back (Fig. 15). Although the cruise back power is low but it takes longer time to reach the destination. In addition, cruise back region has lower voltage, thus increase current drain. Hover and loiter energy consumption is close to each other even the hover time is 2 minutes, it consumes much current.

Transition energy consumption can be reduced if the transition time is lower than present (10 second). In case of the UAV cruise back at the same speed of cruise to target (20 m/s), the energy consumption would increase because in the cruise back region, battery voltage dropped lower than the early time of flight. Therefore, the higher power required higher current drained. For this case, the UAV might not reach the base.

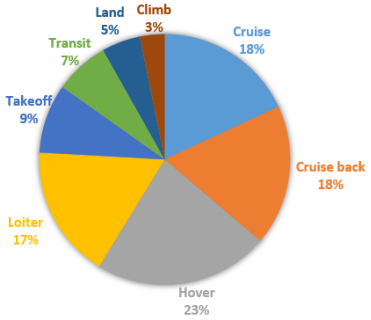

Fig. 15 Energy consumption fraction

The largest power fraction is transition (Fig. 16) because of using fixed wing and multirotor propulsion at the same time. Cruise, cruise back and loiter require electric power 8% and 4% respectively. However, these flight modes use large amount of energy due to the discharged current time.

The multirotor power required of each flight mode were shown in Tables. 11-12. These value will be used as a base to select the motor and rotor size. During takeoff with 3 m/s, power required is higher than hover, thus higher current drain. The effect of vertical takeoff velocity to thrust and power required were discussed in the next section.

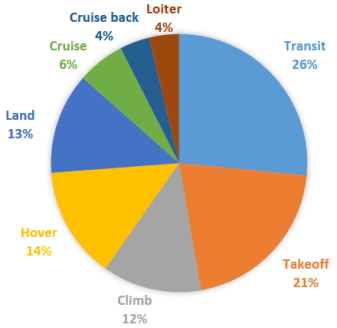

Fig. 16 Electric power required fraction

Table. 11 Power required of multirotor per motor

Parameter name	*Value (W)*
Hover	175
Takeoff	259
Landing	160

Table. 12 Power thrust and weight ratio

$\frac{P_{TO}}{P_H}$	$\frac{P_{LD}}{P_H}$	$\frac{T_{TO}}{W_{TO}}$	$\frac{W_b}{W_{TO}}$	$\frac{W_e}{W_{TO}}$	$\frac{W_{pl}}{W_{TO}}$
1.48	0.90	1.12	0.25	0.53	0.22

5.4 Effect of takeoff velocity

In order to investigate this effect, takeoff velocity was varied from 0.5 to 6 m/s to reach the altitude of 50 m. However, the result shown that the takeoff velocity below 2.5 m/s could not be used because it takes too long time before reaching altitude of 50 m. Therefore, the expected battery capacity was not adequate.

Fig. 17 indicated that higher takeoff velocity, higher thrust and power required. Takeoff weight and drag due to vertical climb affected the thrust and power required. At takeoff velocity of 4.5 m/s, aircraft in multirotor mode requires power 2 times of hover.

Figure of merit of rotor and rotor diameter play a critical role to predict power required. Larger propeller could reduce power required if the same motor weight was used and motor efficiency did not change too much. However, in practice, larger rotor requires more torque, current drain increase to produce more torque which reduce motor efficiency and increase motor case temperature. Then a bigger motor is used instead. Bigger motor, heavier motor weight. If the better motor technology is available and it could be afforded. Lighter motor weight is a good choice to use to reduce the takeoff weight.

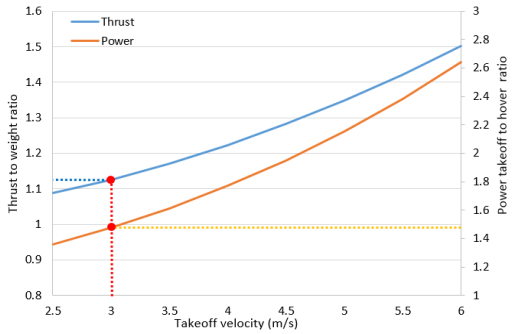

Fig. 17 The effect of takeoff velocity to thrust and power required

In order to investigate each motor power, the multirotor propulsive efficiency was used (Table. 7) to calculate electric power required. Fig. 18 shown the takeoff power and peak current. Battery characteristic was adopted to predict peak current because the higher electric power required, motors consume more current which affected the battery voltage. Higher current drain exists to maintain the power required. The high-C rate battery can be used to reduce this effect. Better propulsive efficiency can reduce the peak current.

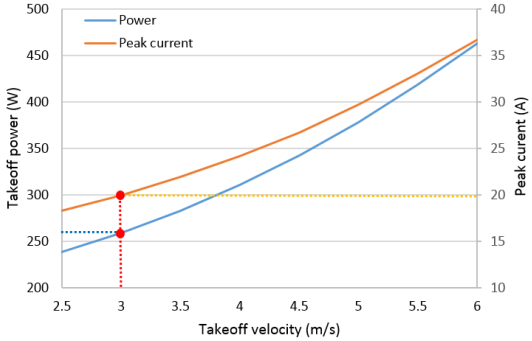

Fig. 18 The effect of takeoff velocity to electric power required and current of each motor

Since the energy consumption depend on both power required and flight time, the energy required (Wh) and discharged current (mAh) were considered as Fig. 19. Takeoff velocity from 2.5-4.5 m/s indicated lower energy required thus lower discharged current. However, faster than 4.5 m/s, energy required increase because this state of discharge current beyond the working condition of the battery. This working condition could damage the battery.

If motor efficiency as the function of current (torque) and motor limit power were taken into account, the takeoff velocity interval that shown lower energy required would be narrower. However, during the conceptual design state these details are unknown.

Designer might use the thrust to weight ratio at desired takeoff velocity to select the rotor and motor from manufacturer or available data.

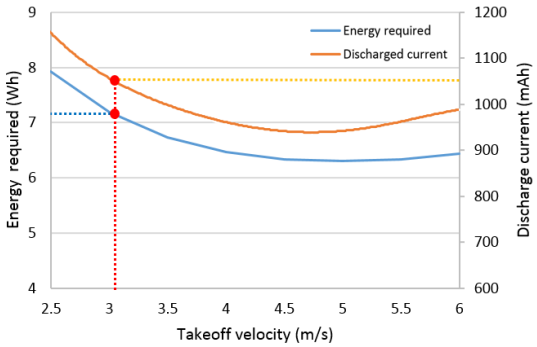

Fig. 19 The effect of takeoff velocity to electric energy required and discharge current

5.4 Energy management

Fixed wing loiter and hover time in the actual situation may differ from the expected flight time (5 minutes for loiter and 2 minutes for hover). Fig. 20 shown the relationship between these two flight mode. The maximum loiter time is 14.5 minutes and maximum hover time is 3.5 minutes. At hover 2 minutes, the loiter time is more than 5 minutes because battery capacity is a little higher than requirement.

This graph can be used as a based during operation. According to safety concern, the maximum discharged capacity before returning to base is 7,500 mAh (usable capacity is 12,000 mAh). In case of without payload during cruise back, higher discharged capacity is acceptable but it is not recommended.

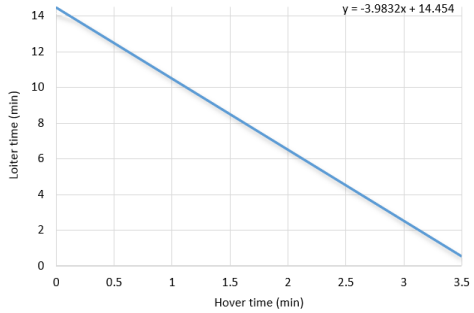

Fig. 20 The relationship between hover and loiter time for standard mission

6. Conclusion and recommendation

This study presented the conceptual design of hybrid fixed wing VTOL UAV. Fixed wing thrust and multirotor thrust were separated to reduce the risk of tilting rotor system failure. Flying wing with coaxial rotor propulsion is the intended platform. The result shown that multirotor system drag has a large fraction of total drag. The stopped rotors orientation should be minimum drag. However, the deep analysis in this extra drag must be performed by CFD, wind tunnel or flight test. If the lower drag were occurred, operating range might increase or reduce the battery weight. The thrust loss of coaxial rotor need to be investigated more details to improve multirotor performance.

The power constant method was utilized to estimate the battery capacity. The result indicated that the voltage constant method tended to underestimate. However, the propulsive efficiency and battery characteristic must be known. Available program for motor selection and matching such as eCalc and motoCalc could be used to help the designer to reach these data.

The increasing takeoff velocity is possible to reduce the energy consumption if the proper motor and rotor were used. The extra weight of multirotor system could be reduced if the high technology motor were used. Motor characteristic must be taken into account.

Energy consumption must be managed properly especially loiter, hover and return to base flight mode.

The next step is select the appropriate airfoil and wing geometry as well as stability analysis. Propulsive efficiency both fixed wing and multirotor and aerodynamic parameters must be investigated to obtain a better range and endurance estimation. The optimization of fixed wing and multirotor system is very much need. Build the prototype to verify the prediction and search for the hidden problems.

7. References

[1] H.C.M. Veerman B.Sc. (2012). Preliminary Multi-Mission UAS Design. M.S. thesis, Delft University of Technology, Netherland.

[2] Spyridon G. Kontogiannis, John A. Ekaterinaris (2013). Design, performance evaluation and optimization of a UAV, Aerospace Science and Technology, vol.29, April 2013, pp. 339–350.

[3] AeroVironment, *UAS: RQ-11B Raven*, URL: https://www.avinc.com/uas/small_uas/raven, accessed on 20/08/2016.

[4] RAFAEL Advanced Defense System, *SKYLITE-B*, URL: http://www.rafael.co.il/Marketing/334-919-en/Marketing.aspx, accessed on20/08/2016.

[5] AVIA.PRO, *ZALA 421-04M*, URL: http:en.avia.pro/blog/zala-aero-zala-421-04m, accessed on20/08/2016.

[6] Hakki Karakas, Emre Koyuncu, Gokhan Inalhan (2012). ITU Tailless UAV Design, *Journal of Intelligent and Robotic Systems*, vol. 69, July 2012, pp. 131–146.

[7] Adnan S. Saeed, Ahmad Bani Younes, Shafiqul Islam, Jorge Dias, Lakmal Seneviratne, Guowei Cai (2015). A Review on the Platform Design, Dynamic Modeling and Control of Hybrid UAVs, paper presented in *International Conference on Unmanned Aircraft Systems (ICUAS) 2015*, Colorado, USA

[8] Ugur Ozdemir, Yucel Orkut Aktas, Karaca Demirbag, Ahmet Erdem (2013). Design of a Commercial Hybrid VTOL UAV System**,** paper presented in *International Conference on Unmanned Aircraft Systems (ICUAS) 2013*, Georgia, USA.

[9] BirdEyeView Aerobotices, FireFLY6 PRO, URL: https://www.birdseyeview.aero/products/firefly6, accessed on 20/08/2016.

[10] Amazon, Amazon Prime Air, URL: https://www.amazon.com, accessed on20/08/2016.

[11] Canberra UAV Open Source Civilian UAV Development, Canberra UAV, URL: http://canberrauav.org.au/, accessed on 20/08/2016.

[12] KU Leuven, Belgium, Students Build drone for Transporting Packages, URL: http://www.kuleuven.be/ , accessed on 20/08/2016

[13] [7] M. Aksugur and G. Inalhan (2010). Design methodology of a hybrid propulsion driven electric powered miniature tailsitter unmanned aerial vehicle, *Journal of Intelligent and Robotic Systems*, vol. 57, September 2009, pp. 505–529.

[14] Delft University of Technology, Netherland, Ambulance Drone,URL: http://www.io.tudelft.nl, accessed on 20/08/2016.

[15] New Atlas, Drones take medical samples to the sky inMadagascar, URL: http://newatlas.com/drones-samples-madagascar/44799/, accessed on 20/08/2016.

[16] National Institute for Emergency Medicine (2014). *Annual report 2014.*

[17] Erdal TORUN (2000). UAV Requirements and Design Consideration, Technical & Project management Department, Turkish Land Forces Command, 06100, Yucetepe, Ankara/TURKEY

[18] Roskam, J. (1997). Airplane Design. Part 1. Preliminary Sizing of Airplanes. Design, Analysis and Research CorporationARcorporation.

[19] Austin, R. Unmanned Aircraft Systems, Aerospace Series, John Wiley&Sons, Ltd., Publication, Chichester, 2010.

[20] Analiza Abdilla, Arthur Richards, Stephen Burrow (2015). Power and Endurance Modelling of Battery-Powered Rotorcraft, paper presented in 2015 IEEE/RSJ International Conference on Intelligent Robots and Systems (IROS), Hamburg, Germany.

[21] Tan Chang, Hu Yu. (2014). Improving Electric Powered UAVs' Endurance by Incorporating Battery Dumping Concept, Procedia Engineering, vol.99, 2015, pp. 168 – 179.

[22] Ohad Gur, Aviv Rosen (2009). Optimizing Electric Propulsion Systems for Unmanned Aerial Vehicles, *Journal of Aircraft*, Vol. 46, no. 4, July–August 2009, pp. 1340-1353.

[23] Lance W. Traub (2016). Calculation of Constant Power Lithium Battery Discharge Curves, *Batteries*, Vol. 2, no. 2, July 2016.

[24] John D. Anderson (1998). Aircraft Performance and Design, McGraw-Hill Education.

[25] Raymer. (2006). Aircraft Design: A Conceptual Approach, Fourth Edition, American Institute of Aeronautics and Astronautics, Inc.

[26] Hoerner, S. F. (1965). Fluid Dynamic Drag, Hoerner Fluid Dynamics, Bakersfield, CA.

[27] Dennis Trips. (2010). Aerodynamic Design and Optimization of a Long Range Mini UAV, M.S. thesis, Delft University of Technology, Netherland.

[28] Shevell, R. S**.** (1989). Fundamentals of Flight. Prentice–Hall, Upper Saddle River, NJ.

[29] Ohad Gur, William H. Mason, and Joseph A. Schetz. (2010). Full-Configuration Drag Estimation**,** *Journal of Aircraft*, Vol.47, no. 4, July–August 2010, pp. 1356-1367.

[30] Gordon J. Leishman (2006). Principles of Helicopter Aerodynamics**,** 2nd Edition, Cambridge University Press.

[31] Bo Wang, Zhongxi Hou, Zhaowei Liu, Qingyang Chen, Xiongfeng Zhu (2016). Preliminary Design of a Small Unmanned Battery Powered Tailsitter, *International Journal of Aerospace Engineering*, Vol. 2016, Article ID 3570581.

[32] David Lundström (2012). Aircraft Design Automation and Subscale Testing, Dissertations, no. 1480, Linköping University, SE-581 83 Linköping, Sweden.

[33] Matthew H. McCrink, James W. Gregory (2015). Blade Element Momentum Modeling of Low-Re Small UAS Electric Propulsion Systems, paper presented in *33rd AIAA Applied Aerodynamics Conference 2015*, Texas, USA.

[34] Silvestre, M.A.R., Morgado, J., Alves, P., Santos, P., Gamboa, P., and Páscoa, J.C. (2015). Propeller Performance Measurements at Low Reynolds Numbers, *International Journal of Mechanics*, Vol.9, 2015.

[35] John B. Brandt, Michael S. Selig. (2011). Propeller Performance Data at Low Reynolds Numbers, paper presented in *49th AIAA Aerospace Sciences Meeting 2011*, Orlando, USA.

[36] Robert W. Deters and Michael S. Selig. (2008). Static Testing of Micro Propellers, paper presented in *26th AIAA Applied Aerodynamics Conference 2008*, Hawaii, USA.

[37] Yao Lei, Yue Bai, Zhijun Xu , Qingjia Gao, Changjun Zhao (2012). An experimental investigation on aerodynamic performance of a coaxial rotor system with different rotor spacing and wind speed, *Experimental Thermal and Fluid Science 44 (2013)*, October 2012, pp. 779–785.

[38] Roman Czyba, Grzegorz Szafranski, Marcin Janik, Krzysztof Pampuch and Michal Hecel. (2015). Development of Co-Axial Y6-Rotor UAV-Design, Mathematical Modeling, Rapid Prototyping and Experimental Validation, paper presented in

International Conference on Unmanned Aircraft Systems (ICUAS) 2015, Colorado, USA.

[39] D. Lundström, K. Amadori, P. Krus. (2010). Validation of Models for Small Scale Electric Propulsion Systems, paper presented in *48th AIAA Aerospace Sciences Meeting Including the New Horizons Forum and Aerospace Exposition 2010*, Orlando, Florida.

[40] T-Motor Safetest Propulsion System, Products, URL: http://www.rctigermotor.com, accessed on 20/08/2016.

[41] Joachim Schömann. (2014). Hybrid-Electric Propulsion Systems for Small Unmanned Aircraft, Ph.D. thesis, Technical University of Munich, Germany.